Unveiling spatial and temporal heterogeneity of a tropical forest canopy using high-resolution NIRv, FCVI, and NIRvrad from UAS observations

Trina Merrick[1,4,8*], Stephanie Pau[1], Matteo Detto[2,3], Eben N. Broadbent[4], Stephanie. A. Bohlman[2,5], Christopher J. Still[6], Angelica M. Almeyda Zambrano[7]

[1] Department of Geography, Florida State University, 113 Collegiate Loop, Tallahassee, Florida 32306, USA
[2] Smithsonian Tropical Research Institute, Apartado 0843–03092, Balboa, Ancon, Panama
[3] Department of Ecology and Evolutionary Biology, Princeton University, Princeton, New Jersey 08544 USA
[4] Spatial Ecology and Conservation Lab, School of Forest, Fisheries and Geomatics Sciences, University of Florida, Gainesville, FL, 32608 USA
[5] School of Forest, Fisheries and Geomatics Sciences, University of Florida, Gainesville, FL, 32608 USA
[6] Department of Forest Ecosystems and Society, Oregon State University, Corvallis, Oregon 97331 USA
[7] Spatial Ecology and Conservation Lab, Center for Latin American Studies, University of Florida, Gainesville, Florida 32608 USA
[8] Naval Research Laboratory, Remote Sensing Division, 4555 Overlook Ave. SW, Washington, DC, 20375, USA

Author's current location

Correspondence to: Trina Merrick (trina.merrick@nrl.navy.mil)

Abstract. Recently, remotely-sensed measurements of the near-infrared reflectance (NIRv) of vegetation, the fluorescence correction vegetation index (FCVI), and radiance (NIRvrad) of vegetation, have emerged as indicators of vegetation structure and function with potential to enhance or improve upon commonly used indicators, such as the normalized difference vegetation index (NDVI) and the enhanced vegetation index (EVI). The applicability of these remotely sensed indices to tropical forests, key ecosystems for global carbon and biodiversity, have been limited. In particular, fine-scale spatial and temporal heterogeneity of structure and physiology may contribute to variation in these indices and the properties, such as gross primary productivity (GPP) and absorbed photosynthetically active radiation (APAR), that are presumed to be measured by these indices. In this study, fine-scale (15cm and greater) tropical forest heterogeneity represented by NIRv, FCVI, and NIRvrad, is investigated using unoccupied aerial systems (UAS) data, and compared to NDVI, EVI, and Lidar. By exploiting near-infrared signals, emerging vegetation indicators captured the greatest spatiotemporal variability, followed by the enhanced vegetation index (EVI), then the normalized difference vegetation index (NDVI). Wavelet analyses showed the dominant spatial scale of variability of all indicators is driven by tree clusters and larger-than-tree-crown size gaps rather than individual tree crowns. Emerging indices and EVI captured variability at smaller spatial scales (~50 m) than NDVI (~90 m) and lidar (~70 m). We show that spatial and temporal patterns of NIRv and FCVI are virtually identical for a dense green canopy, confirming predictions in earlier studies. Furthermore, we show that NIRvrad, which does not require separate irradiance measurements, correlated more strongly with GPP and PAR than did other indicators. These emerging indicators, which are related to canopy structure and the radiation regime of vegetation canopies, are promising tools to improve understanding of tropical forest canopy structure and function.

1 Introduction

Important spatial and temporal heterogeneity in structurally complex and species-rich tropical forests are not well characterized. Many factors, including varying microclimate, light conditions, topography, crown structure, and patterns of tree mortality and regeneration, contribute to high heterogeneity that underlies coarse scale gross primary production (GPP) measurements in tropical forest (e.g., Xu et al., 2015; Guan et al., 2015; Morton et al., 2014; Bohlman and Pacala, 2012; Laurance et al., 2012; Clark et al., 2008; Huete et al., 2008). Improving knowledge of tropical forest dynamics at multiple scales is crucial to monitoring and predicting resilience of tropical ecosystems and productivity under climate change (Liu et al., 2021; Clark et al., 2017; Laurance et al., 2012; Malhi, 2012; Wright, 2010; Saatchi et al., 2010; Lewis et al., 2009). Remote sensing (RS) measurements have been employed to uncover vegetation patterns of structure and productivity from local to global scales, often with a focus on filling gaps in knowledge regarding variation and uncertainties in GPP estimates (e.g., Jung et al., 2011; Glenn et al., 2008; Huete et al., 2002; Ryu et al., 2018; Yang et al., 2017; Jiang et al., 2008; Zhao et al., 2010; Heinsch et al., 2006; Running et al., 2004; Turner et al., 2003). Yet, there is a spatial mismatch between satellite data (e.g., 30 m to 1 km pixel resolution), which provides observations across large extents at repeat intervals, and site-specific plot level data (e.g., $0.1 - 1$ hectare) that contributes to uncertainties in GPP estimates (Gelybó et al., 2013; Zhang et al., 2020). There is a lack of high spatial and temporal resolution data that can capture fine-grained heterogeneity of tropical forests (Clark et al., 2017; Mitchard, 2018; Saatchi et al., 2011; Lewis et al., 2009). Unoccupied aerial systems (UAS) with hyperspectral imaging sensors present an opportunity to collect tropical forest canopy data at high spatial resolution, which could address unknowns related to the high heterogeneity of tropical forests.

Traditional reflectance-based indices (RI) using RS data, such as the normalized difference vegetation index (NDVI) and enhanced vegetation index (EVI), are known to capture structural changes that are coincident with changes in GPP. RIs have provided optical methods using RS to track GPP via the light use efficiency (LUE) model (J.L.Monteith, 1977; Yuan et al., 2014; B. E. Medlyn, 1998). In the most commonly used formulation of the LUE model for RS, GPP is the product of the absorbed photosynthetically active radiation (APAR) and the efficiency (ε) with which the target vegetation converts the radiation to carbon (Gamon, 2015;Yuan et al., 2014; Running et al., 2004). APAR is derived from the incoming photosynthetically active radiation (PAR) times the fraction of PAR (fPAR). RIs commonly used in the LUE model of GPP as well as direct proxies for GPP are NDVI and EVI, because of a strong relationship to fPAR (Springer et al., 2017; Morton et al., 2015; Gamon et al., 2015; Porcar-Castell et al., 2014; Glenn et al., 2008; Gao et al., 2007; Huete et al., 2002; Zarco-Tejada et al., 2013). NDVI and EVI are typically used as proxies on seasonal timescales, or, when used to examine changes on shorter timescales, they have been multiplied by photosynthetically active radiation (PAR) to account for changes in radiation (incoming, absorbed, and scattered) which better align with GPP changes (Springer et al., 2017; Yuan et al., 2014). However, RIs alone have often not shown enough sensitivity to capture more fine-scale or rapid changes in vegetation, such as those in tropical forests, and questions linger about the ability to track green-up with RIs in tropical regions (Liu et al., 2021; Yang et al., 2018a; Lee et al., 2013; Xu et al., 2015; Morton et al., 2014; Samanta et al., 2010; Sims et al., 2008).

Recently, three emerging vegetation indicators have been shown to track with GPP more closely than traditional RIs. These indicators are the near-infrared reflectance of vegetation (NIRv) (Badgley et al., 2017), the fluorescence

74 correction vegetation index (FCVI) (Yang et al., 2020) and the near-infrared radiance of vegetation (NIRvrad) (Wu et

75 al., 2020). Because they exploit additional information from the NIR region of the spectrum, NIRv, FCVI, and

76 NIRvrad do not saturate in dense canopies or suffer the same level of contamination from senesced vegetation and

77 soils as traditional RIs (Baldocchi et al., 2020; Badgley et al., 2017). Additionally, these emerging indicators require

78 only moderate spectral resolution data and are similarly straightforward to measure and calculate as RIs, making them

79 accessible in a broad range of studies. In contrast, SIF measurements require very high spectral resolution and multiple

80 instruments. Therefore, NIRv, FCVI, and NIRvrad could be employed as valuable indicators of canopy structure and

81 function (Badgley et al., 2019; Badgley et al., 2017; Dechant et al., 2020) and have practical advantages over making

82 SIF measurements.

83   NIRv, the product of NDVI and the near-infrared reflectance (NIR), from moderate spectral resolution

84 satellite imagery and field spectrometers has been shown to empirically track measured and modelled GPP globally

85 (with highest uncertainties in the tropics) at monthly to seasonal timescales presumably because changes in canopy

86 phenology influence light capture and these changes coincide with changes in GPP (Badgley et al., 2019; Badgley et

87 al., 2017; Dechant et al., 2020). FCVI, derived from radiative transfer theory rather than an empirical relationship, is

88 calculated from RS data by subtracting the reflectance in the NIR from the reflectance in the visible range (Yang et

89 al., 2020). Yang et al. (2020) demonstrated that FCVI, by capturing structure and radiation information from a

90 vegetated canopy, tracked GPP and solar-induced fluorescence (SIF; a radiance-based indicator of GPP) in field

91 experiments with crops and in numerical experiments. Yet FCVI showed differences from NIRv due to exposed soil

92 within the vegetated study areas. In previous studies, FCVI and NIRv were similar for dense green canopies where

93 soils have less of an impact, but this has not yet been tested in the tropics (Wang et al., 2020; Badgley et al., 2019;

94 Dechant et al., 2020). NIRvrad was proposed as a proxy for GPP on half-hourly and daily timescales, in contrast to

95 NIRv and FCVI which track changes on longer timescales (Wu et al., 2020; Dechant et al., 2020; Baldocchi et al.,

96 2020; Zeng et al., 2019). NIRvrad is calculated by multiplying NDVI by the NIR radiance, and because the radiance

97 of NIR accounts for incoming radiation at short timescales, has tracked GPP and SIF on half-hourly and diurnal scales

98 as well as seasonally in crops and, to a limited extent, natural grass and savanna ecosystems (Dechant et al., 2020;

99 Baldocchi et al., 2020; Zeng et al., 2019; Wu et al., 2020).

100   Readily available UAS-based hyperspectral sensors are capable of robust measurements of NIRv, FCVI, and

101 NIRvrad at ultra-high spatial scales, i.e. in tens of centimeters. In this regard, UAS-based data have the potential to

102 improve our understanding of tropical forest structure and function over a range of scales that are poorly resolved by

103 other RS platforms. Here, we use high spatial resolution UAS measurements to characterize spatial and temporal

104 variation in a semi-deciduous tropical forest canopy during the dry season, and compare commonly used spectral

105 indices (NDVI and EVI) to newer vegetation indicators (NIRv, NIRvrad, and FCVI) by (i) examining correlations

106 between GPP and vegetation indicators using mean values across the canopy throughout the day, (ii) evaluating the

107 distribution of fine spatial resolution values (~15 cm) across the canopy and examining changes in this spatial variation

108 throughout the course of two days, and finally (iii) identifying the dominant spatial scale driving variation across our

109 10 ha study region.

2   Materials and Methods

2.1 Study Area

Barro Colorado Island (BCI), Panama, is a 1560 ha island (approximately 15 km^2) in Gatun Lake, which was formed by the construction of the Panama Canal. The Smithsonian Tropical Research Institute manages the preserved area specifically for research. This semi-deciduous moist tropical forest receives approximately 2640 mm mean annual precipitation and has a mean temperature of 26ºC with a dry season from approximately January through April (Detto et al., 2018). There is high species diversity, with approximately 500 tree species, approximately 60 species per ha, and about 6.3% of trees at >30cm diameter at breast height (dbh) (Bohlman and O'Brien, 2006; Condit et al., 2000). The UAS and ground measurements were focused on an area approximately 10 ha within the footprint of an eddy covariance tower near the center of the island (9.156440°, -79.848210°).

2.2 Data collection

The GatorEye Unmanned Flying Laboratory is a hardware and software system built for sensor fusion applications, and which includes hyperspectral, thermal, and visual cameras and a Lidar sensor, coupled with a differential GNSS, internal hard drives, computing systems, and an Inertial Motion Unit (IMU). Hardware and processing details, as well as data downloads, are available at www.gatoreye.org. The GatorEye flew 13 missions on January 30 and 31, 2019 over the forest canopy within the eddy covariance tower footprint at an average height of 120 m above ground level (AGL) and at 12 m/s (Fig. 1). In this study, we used radiometrically calibrated flight transects from the Nano VNIR 270 spectral band hyperspectral sensor (Headwall Photonics, Fitchburg, MA, USA) which covered approximately 1 ha per flight within the EC footprint in this study. The Nano spectrally samples at approximately 2.2 nm and 12-bit radiometric resolution from 400 to 1050 nm. The frame rate was set to 100 fps, with an integration time of 12 ms and provided a pixel resolution of approximately 15x15 cm. The Nano was calibrated to radiance by the manufacturer before the field campaign and pixel drift was removed by dark images collection, which was corrected for during the conversion from digital number to radiance. The hyperspectral transects were equally subset for each flight in ENVI + IDL (Harris Geospatial, Boulder, CO). Each flight resulted in 1920 transects of approximately 400 m length composing three blocks discretized in 2500 data points. Simultaneous lidar was collected using a VLP-32c ultra puck (Velodyne, San Jose, CA), which was processed to a 0.5x0.5 m resolution digital surface model (DSM).

Turbulent fluxes and meteorological variables were measured from a 40 m Eddy Covariance (EC) flux tower (Fig. 1). The eddy covariance system includes a sonic anemometer (CSAT3, Campbell Scientific, Logan, UT) and an open-path infrared CO_2/H_2O gas analyzer (LI7500, LiCOR. Lincoln, NE). High-frequency (10Hz) measurements were acquired by a datalogger (CR1000, Campbell Scientific) and stored on a local PC. Other measurements made at the tower include air temperature and relative humidity (HC2S3, Rotronic, Hauppauge New York), and photosynthetically active radiation (PAR; BF5, Delta-T Devices, UK). EC data were processed with a custom program using a standard routine described in Detto et al. (2010). GPP was derived from daytime values of NEE by adding the corresponding mean daily ecosystem respiration obtained as the intercept of the light response curve (Lasslop et al.,

145 2010). Due to a power issue, data corresponding to the January 30 flights was not collected, so only January 30 GPP

146 were available.

147   An HH2 Pro Spectroradiometer (HH2; ASD/Panalytical/Malvern, Boulder, CO) fitted with a diffuse cosine

148 receptor was used on the ground in full sun at the forest edge to record incoming irradiance on January 30 and 31,

149 2019 (~ 3nm FWHM and spectral sampling at 1nm). HH2 irradiance was resampled to match the Nano hyperspectral

150 sensor and used to calculate reflectance. A calibrated reference tarp was placed in full sun at the forest edge and the

151 UAS flew over and recorded the tarp each UAS flight. Reflectance was calculated separately using the HH2 and tarp

152 data and resulting reflectance values compared as a method to vicariously cross-calibrate reflectance from the

153 hyperspectral data (<7.0% difference for all data in the study). In addition, PAR was calculated with the HH2 data and

154 compared to the tower-mounted PAR measurement (approximately 1.5 km apart) to help understand any differences

155 in the sky conditions during flight times. PAR differences across the site for each flight time for the duration of flights

156 (approximately 10-15 minutes in length each) ranged between 4.0% and 10.3%. A summary of materials and methods

157 is provided in Fig.1 at the end of Section 2.

158

2.3 Vegetation indicators

159

160 We calculated NDVI and EVI as (Tucker, 1979; Huete et al., 2002; Rouse JR et al., 1974):

$$NDVI = \frac{R_{770-800} - R_{630-670}}{R_{770-800} + R_{630-670}} \tag{1}$$

161 and

$$EVI = \frac{2.5(R_{770-800} - R_{630-670})}{R_{770-800} + 6 \times R_{630-670} - 6 \times R_{460-475} + 1} \tag{2}$$

162 where R is reflectance and the subscripts indicate wavelengths. Here, we used the averages of 770-800 nm for NIR,

163 630-670 nm for red reflectance, and 460-475 nm for blue bands reflectance and normalized to reduce noise.

164 We further calculated the near-infrared vegetation index NIRv as:

$$NIRv = NDVI \times R_{770\text{-}800} \tag{3}$$

165 where R770-800 is the NIR reflectance (Badgley et al., 2017). The fluorescence correction vegetation index (FCVI)

166 was calculated from spectral data by subtracting the reflectance in the visible range (R400-700) from the NIR

167 reflectance (Yang et al., 2020) as follows

$$FCVI = R_{770\text{-}800} \text{-} R_{400\text{-}700} \tag{4}.$$

168 The near-infrared radiance of vegetation (NIRvrad) was calculated similarly to the NIRv, except NDVI was multiplied

169 by the radiance, rather than reflectance, from the NIR region (Rad770-800) (Wu et al., 2020) as follows:

$$NIRvrad = NDVI \times Rad_{770\text{-}800} \tag{5}.$$

2.4 Data Analysis

170

171   We examined mean values across the canopy over the course of one day by creating a diurnal time series of

172 scatterplots of the tower-based PAR data, tower-based GPP data, and means of all spectral vegetation indicators, on

173   Jan 31, 2019, and ran comparisons using Pearson's correlation coefficients to examine correlations. At fine spatial

174   scales, i.e. pixel level of ~15 cm, we created density plots, calculated the coefficient of variation (CV), and calculated

175   the means of all vegetation indicators (NDVI, EVI, NIRv, FCVI, NIRvrad) for each flight to compare spatial and

176   temporal variability (Fig. 1). To determine which spatial scales dominate the variability of each vegetation quantity,

177   we ran power spectrum wavelet analysis using code created in the Matlab programming language (Mathworks, Natick,

178   Massachusetts). For each vegetation quantity and each flight, and for the lidar elevation model representing canopy

179   height, we computed the Morlet wavelet power spectrum of individual transects (Torrence and Compo, 1998). All

180   power spectra from the wavelet analysis were normalized to unit variance. An ensemble power spectrum for each

181   vegetation indicator was created by averaging across all the transects of each flight and then across flights. We then

182   compared the power spectra for each vegetation indicator and lidar data to compare the spatial scales at which the

183   quantities captured variability as well as the spatial scale at which the lidar-based elevation model captured variability.

184   For illustration purposes, Fig. S3 is an example of two signals, a higher and lower noise signal created with fractals

185   (Signal A and B, respectively, Fig. A1) and the corresponding power spectra which decay differently at smaller spatial

186   scales (Power Spectra, Fig. A1). Initial UAS data processing was carried out in Interactive Data Language (IDL) and

187   Environment for Visualizing Images (ENVI) (Harris Geospatial, Boulder, CO). Other analysis, including graphical

188   illustrations, were carried out using the R open source environment with libraries dplyr, ggplot, and tidyverse (R

189   Development Core Team, 2010; Wickham et al., 2018; Wickham, 2017, 2016) and Matlab (Mathworks, Natick,

190   Massachusetts).

191
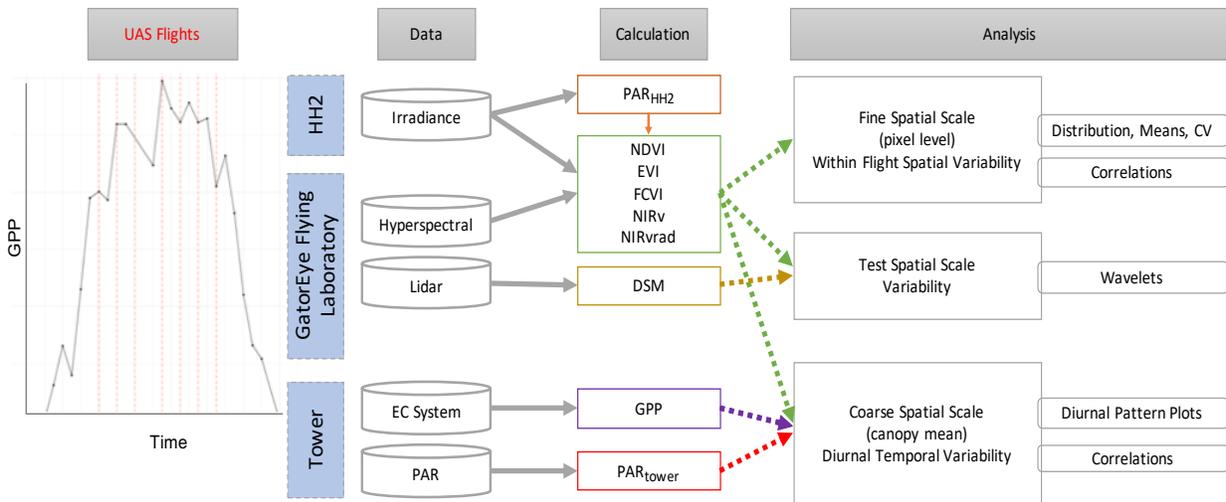
192

193   **Figure 1.** **Summary of methods. Concept of diurnal GPP and UAS flights (far left).** **Platforms and instrumentation (blue)**
194   **consisted of the Analytical Spectral Devices (ASD) Handheld Spectroradiometer Pro 2 (HH2), the GatorEye Flying**
195   **Laboratory, and the Tower at Barro Colorado Island (BCI). Data collected included Irradiance, Hyperspectral, Lidar,**
196   **Eddy Covariance System (EC), and Photosynthetically Active Radiation (PAR). Calculations made were PAR with the HH2**
197   **(PARHH2), the Normalized Difference Vegetation Index (NDVI), Enhanced Vegetation Index (EVI), Fluorescence**
198   **Correction Vegetation Index (FCVI), the Near Infrared Vegetation Index (NIRv), the Near Infrared Radiance of Vegetation**
199   **(NIRvrad), the Digital Surface Model (DSM), Gross Primary Productivity (GPP) and PAR from the PAR Sensor on the**
200   **Tower (PARtower). An overview of the data analysis at each scale is provided in the right of the diagram.**

3 Results and discussion

3.1 Diurnal trend in spectral vegetation indicators, PAR, and GPP

The degree to which remote sensing vegetation indicators represent changes in GPP depend largely on canopy structure-dependent light absorption and scattering processes, that is, a joint relationship between a remote sensing vegetation quantity, PAR or APAR, and GPP. Fig. 2 shows GPP, PAR, and the mean value of each vegetation quantity at each flight time over the course of January 31, the day on which we had overlapping data between the UAS and eddy covariance system (Fig. 2a-d). Additionally, Pearson correlation coefficients among mean NIRv, FCVI, NIRvrad, EVI, and NDVI for each flight time and the GPP and PAR values at the flight times are shown in Fig. 2d. NIRv is significantly and strongly positively correlated to both FCVI (r=0.9, p<0.001) and EVI (r=0.9, p<0.01). NIRvrad is the only vegetation quantity with a significant correlation to PAR and GPP, with a strong positive relationship (0.9 and 0.81, respectively, p-values <0.05; Fig. 2d). Mean NIRvrad values also have the greatest relative diurnal change among the vegetation indicators (Fig. 2c and d). These results demonstrate that a shared correlation of NIRvrad and GPP to PAR results in mean NIRvrad tracking diurnal changes in GPP to a greater degree than NIRv, FCVI, NDVI or EVI, because NIRvrad takes incoming radiation into account whereas the other vegetation indicators do not. This evidence – albeit based on only one day of data – supports the proposed use of NIRvrad as a proxy for changes in GPP on short timescales. NIRvrad is also a more efficient measurement of GPP in the sense that a separate instrument to measure PAR is not needed (Wu et al., 2020; Zeng et al., 2019). Given that the relationship between NIRvrad and GPP depends on PAR, it is unclear if the association between NIRvrad and GPP would weaken during the wet season when low light or diffuse light conditions are more common (Berry and Goldsmith, 2020).

220
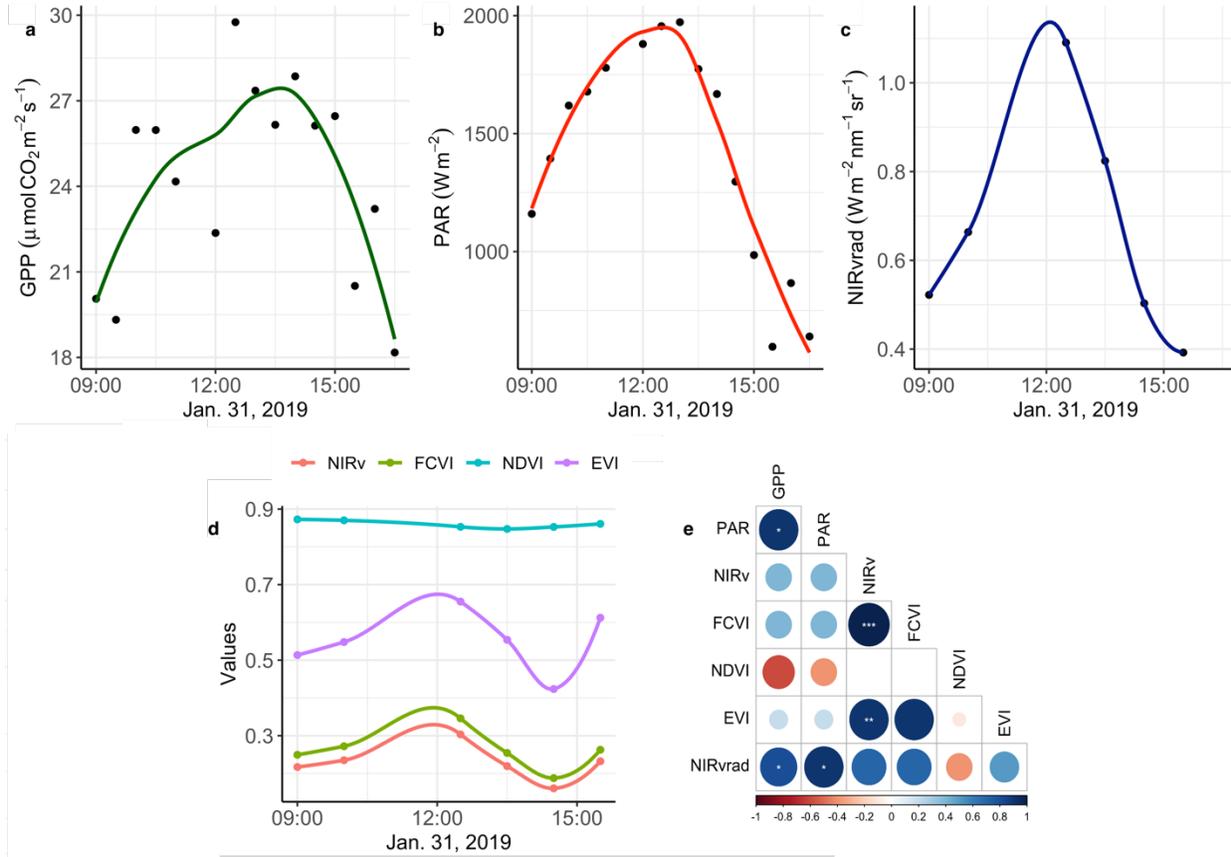
Fig. 2. Diurnal time series of a) GPP b) PAR c) NIRvrad d) NIRv, FCVI, NDVI, and EVI e) comparisons of quantities using Pearson correlations color indicates strength of relationship, * = p-value<0.05, ** = p-value <0.01, *** = p-value <0.001.

3.2 Tropical forest canopy variation

Spatial distributions and CV of all pixels of NIRv, FCVI, and NIRvrad are generally similar to one another and show considerable variation spatially across the canopy and temporally over the course of a day and across days (Fig. 3a-c, Table A2). NIRv, FCVI, and NIRvrad distributions are distinct from EVI and NDVI (Fig. 3a-e, Table A2, and Table A2). NIRv, FCVI, and NIRvrad have the highest CV at each flight time (between 39.78% and 91.54%, Table A1), followed by EVI (between 20.24% and 37.24%, Table A2) and NDVI varied the least at any flight time (between 9.83% and 12.82%, Table A2). For some indices, mean values across the canopy fail to capture extreme high (NIRv, NIRvrad, and FCVI) or low values (NDVI) during morning and afternoon hours. This pattern suggests "hot" and "cool" spots of activity related to heterogeneity in forest structure and low sun angles. In previous studies, the directional effects on NIRv have been examined on coarse spatial scales (i.e. satellites) and have been proposed as a means of improving understanding of NIRv agreement to GPP (Hao et al., 2021; Dechant et al., 2020; Baldocchi et al., 2020; Zhang et al., 2020). Our results demonstrate that NIRv, FCVI, and NIRvrad capture fine-grained heterogeneity of this tropical forest canopy, which was obscured by EVI and NDVI (Fig. 3a-e). NIRv and NIRvrad use NDVI, thus, by definition, NIR is the largest contributing factor to the heterogeneity captured (Fig. 3a, c, and e). While NIRv and NIRvrad distributions are generally similar, they diverge in the afternoons when PAR declines, which likely why NIRvrad is better correlated with GPP. EVI variability was higher than NDVI variability, but lower than

that of NIRv, FCVI, and NIRvrad, indicating that EVI has a different level of sensitivity to viewing geometry and canopy components (potentially understory), light absorption and scattering regime of the canopy than the other indices (Table A1and Table A2). We also show empirically that NIRv and FCVI are virtually the same in a dense tropical forest presumably due to both indices similarly representing the radiation regime of the tropical forest canopy, i.e. light capture and scattering, in conditions with little background soil, supporting the predictions of earlier studies (Dechant et al., 2020; Zeng et al., 2019; Yang et al., 2018b; Wu et al., 2020).

Midday distributions of NIRv, FCVI, and NIRvrad on Jan. 30 at 12:00 and 1330 and Jan. 31 at 12:30 are less skewed than at other times of the day whereas morning and afternoon distributions are skewed toward lower values, except for Jan. 31 at 15:30 (Fig. 3a-c). On both days, when mean values peak at midday, the variation for all vegetation indicators is lowest (Jan 30, 1200 CV between 47.6 and 49.2 and Jan 31, 1230 CV between 45.6 and 47.2) (Fig. 3, Table A1). The highest variability occurred in the afternoon on both days (Jan 30, 1630 CV between 91.3% and 91.5 and Jan 31, 1430 CV between 83.3% and 83.8% for all quantities) (Fig. 3, Table A2). At midday, NIRv, FCVI, and NIRvrad variability was low and means were high, indicating that viewing and sun geometry drive the higher and lower values during morning and afternoon. This effect is greater in the afternoon than the morning (Fig. 3, Table A2). However, a different pattern is apparent on Jan. 31 during the 1530 flight time when mean values increased from the 1430 flight time means and the CV values were the lowest of any flight observations in the study and this influence appears to be greatest on EVI. It is possible that this was due to another type of effect on illumination geometry, such as wind influencing the UAS, diffuse radiation effects, or hotspot effects.
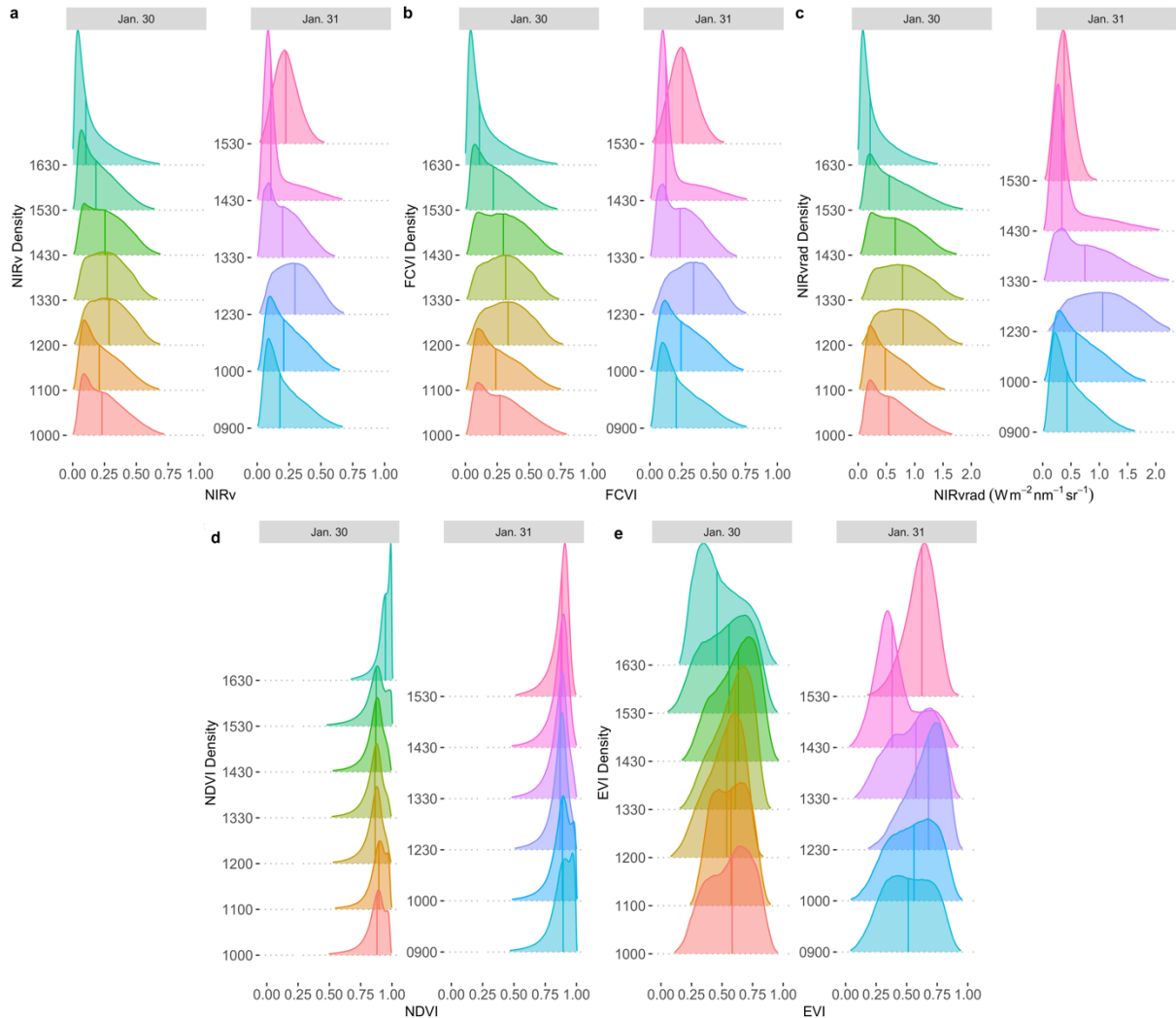
Fig. 3. NIRv (a), FCVI (b), and NIRvrad (c) density plots for each flight time on January 30, 2019 (column 1each panel) and January 31 (column 2 each panel). Colours of distributions indicate the flight time and day.

3.3 Power Spectrum Analysis

Power spectrum analysis was used to identify the dominant spatial scales driving variability across the canopy (Fig. 4). In Fig. 4, the area beneath the curve is proportional to the variance because it is the spectrum divided by the corresponding scale and then plotted as a function of the log of the scale (example signals and power spectra provided Fig. A1). Similar to their spatial distributions (Fig. 3), NIRvrad and FCVI are indistinguishable in their dominant scales of spatial variability (Fig. 3) (Dechant et al., 2020; Zeng et al., 2019). Power spectrum analysis shows a distinct peak around 50 m spatial scale for NIRv, NIRvrad, FCVI, and EVI, whereas NDVI peaks at approximately 90 m. The largest tree crown sizes on BCI are on the order of 20-30 m in diameter and the most common crown sizes are between 4-10 m (Fig. A2). Thus, the spatial variability of the vegetation indicators is strongly influenced by larger forest structures, such as forest gaps and tree clusters, rather than individual tree crowns.

This larger scale of variability is also confirmed by the power spectrum of the lidar-derived canopy surface model, which displays a peak at 70 m scale, indicating that larger than tree crown scales produce the most variability

272 in canopy height. In other words, UAS-based lidar data also show that canopy heights within a 70 m spatial scale

273 create strong spatial features on the landscape. Vegetation indicators and the lidar canopy surface model appear less

274 effective at capturing smaller scale differences within a canopy (leaves or leaf clumps) or among the most frequent

275 tree crown sizes on BCI (4-10 m sunlit tree crown sizes determined by stereophotos; Fig. A2). However, the peaks in

276 the vegetation indicators are broader than the peak in the lidar data, showing that smaller features of the canopy are

277 still contributing to the total spatial signal in the power spectra. These results suggest that satellite data with a spatial

278 resolution greater than ~50 m may miss important variation in diverse tropical forest canopies. NDVI displays a

279 different shape with a slower decay at small scales, indicating less distinguishable spatial structures from the canopy,

280 and a peak shifted to the larger scales (Fig. 4), i.e. NDVI does not distinguish smaller spatial structures. At much larger

281 scales (>100-200 m), the vegetation indicators decline smoothly, while NDVI and especially lidar show an increase

282 in variance probably associated with topographic heterogeneity.

283   One reason why vegetation indicators and LiDAR captured variability at spatial scales larger than the most

284 common tree crown sizes on BCI is that canopy heights tend to be more uniform on BCI compared to other tropical

285 forests, possibly due to wind (Bohlman and O'Brien, 2006). For example, Dipterocarpus dominated South-East Asian

286 forests have emergent trees, unlike BCI, which can reach up to 60 m in height. Additionally, tree crowns on BCI tend

287 to be more flat-topped than conical or rounded, and trees can be found clumped in similar heights, which could explain

288 why the most often detected unit is larger than the mean of a single crown. On the other end of the spectrum, forest

289 gaps can be larger than a single crown because treefall often affects neighbouring trees.

290   Vegetation indicators and the Lidar-derived surface model represent the spectral and structural properties most

291 broadly of the upper canopy, and thus it is conceivable that they display similar spatial variability. However, NIRv,

292 FCVI, NIRvrad, and EVI discriminated details at a different spatial scale from NDVI and LiDAR. These results

293 parallel the variability detected in their distributions (Fig. 3 and Table A1), where NDVI patterns were distinct from

294 the other vegetation indicators. Taken together, these results show that NIRv, FCVI, and NIRvrad have a smoother

295 spatial pattern and peak at finer scales than NDVI, which is known to saturate at high green biomass (Zhu and Liu,

296 2015; Huete et al., 2002), whereas the emerging vegetation indicators should better correlate with aspects of

297 photosynthetic capacity. Thus, these emerging indicators should measure finer resolution spatial heterogeneity and

298 should be more adept at monitoring changes in structure and function of the canopy than NDVI. Additionally, the

299 emerging indicators can potentially disaggregate the physiological and structural component of SIF when SIF

300 measurements are available since changes in structure of the forest coincide with changes in GPP (Wang et al., 2020;

301 Wu et al., 2020; Yang et al., 2020; Dechant et al., 2020). Emerging indicators' heightened ability to differentiate the

302 fine-scale spatial variability in the canopy is likely due to the influence of high upwelling of NIR from the canopy and

303 understory, particularly in the dry season, which tend to blur the signal of the upper canopy for NDVI. Notably, EVI

304 and NDVI, two common indicators of vegetation greenness, show differences in their power spectrum, in particular

305 the slope of the curve for scales less than 20 m. EVI was designed to better capture vegetation changes by exploiting

306 variability in the reflectance in the blue range, especially effective in dense green canopies. This may help explain the

307 scale of variability in this canopy where variation in the blue may be expected to manifest, especially because

308   deciduous crowns, which have high reflectance in blue wavelengths compared to fully leaved crowns, are present on
309   BCI.

310

311
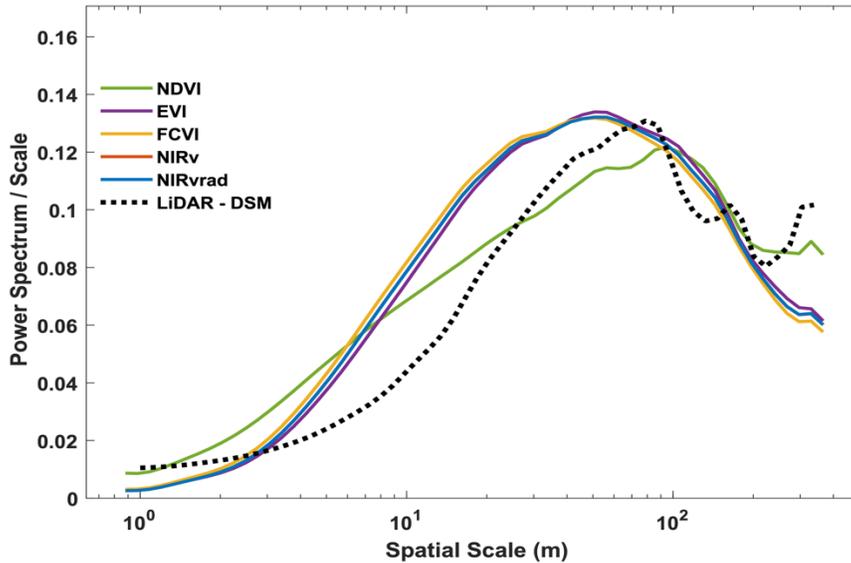
Fig. 4. Ensemble wavelet power spectra for all the quantities used in this study and a LiDAR-derived digital
surface model (DSM). Note that FCVI and NIRv are similar, thus the NIRv curve is obscured by the FCVI.
Ensembles were created by averaging the spectrum of individual transects, then averaging across flights. Note
that in this representation, the spectrum divided by the corresponding scale as a function of the log of the scale,
the area beneath the curve is proportional to the variance.

4   Conclusions

We examined NIRv, FCVI, and NIRvrad, emerging vegetation indicators related to fPAR and the scattering of
SIF photons, of a semi-deciduous tropical forest canopy using UAS-based hyperspectral data. Our findings
demonstrate that NIRvrad has greater potential to track GPP over the course of a day than the non-radiance-based
indices as evidenced by a shared correlation among NIRvrad, PAR, and GPP. Thus NIRvrad is a potential proxy for
tracking GPP on short timescales without the need for separate measurements of incoming irradiance, which SIF
requires. Also, NIRv, FCVI, and NIRvrad at high spatial resolution (~15cm) unveil greater spatial and diurnal
variability of BCI's tropical forest canopy versus EVI or NDVI, which may pave the way to improve our understanding
of the relationship between GPP and remote sensing observations. The dominant scale driving spatial variability of
spectral measurements and lidar data are larger forest structures occurring on BCI, such as groups of similar trees or
forest gaps. Yet, smaller, broader peaks in the power spectra of NIRv, FCVI, NIRvrad, and EVI indicate these four
indices incorporate smaller scale information compared to NDVI. Taken together, the demonstrated potential to track
GPP, measure spatial heterogeneity and variability, and capture forest structural characteristics of BCI open greater
possibilities to examine structure and function within and across this tropical forest.

331   Because remote sensing advancements are making it possible to capture physiological responses of vegetation,
332 the importance of improved techniques to examine the radiation regime, for instance estimating fPAR or APAR, can
333 be overlooked. However, recent studies have highlighted the importance and difficulties of measuring fPAR and
334 APAR, the strong dependence of measurements on illumination and viewing geometry, as well as the need for
335 increased understanding of structure-related radiation regime information more generally e.g. (Hao et al., 2021;
336 Dechant et al., 2020; Baldocchi et al., 2020; Rocha et al., 2021; Zhang et al., 2020). For NIRv, FCVI, and NIRvrad,
337 inclusion of the NIR spectral region makes the emerging indices more sensitive to incoming, absorbed, and scattered
338 radiation, which can be influenced by illumination and viewing geometry, changes in canopy leaf angles or associated
339 structure changes. In the case of NIRvrad, which was most strongly associated with GPP, changes in light regime and
340 associated photosynthetic capacity can even be captured diurnally. This study highlights the importance of
341 understanding the incoming solar radiation, absorbed and scattered radiation, and illumination and viewing geometry
342 of any remote sensing data, but it also encourages exploiting RS observations to improve our ability to measure
343 structure-related light capture and scattering patterns. It is in this role, we show these measurements should be further
344 investigated as valuable tools to improve our understanding of complex tropical forest canopies and potentially as an
345 improved estimate of fPAR, APAR, or GPP. While this study focuses on BCI, these techniques could be applied more
346 broadly for the purposes of defining the dominant scale of spatial variability, tracking structural changes, monitoring
347 coincident changes in GPP or light regime, or as inputs to vegetation models of tropical forest structure and function.

348 **5   Appendix**
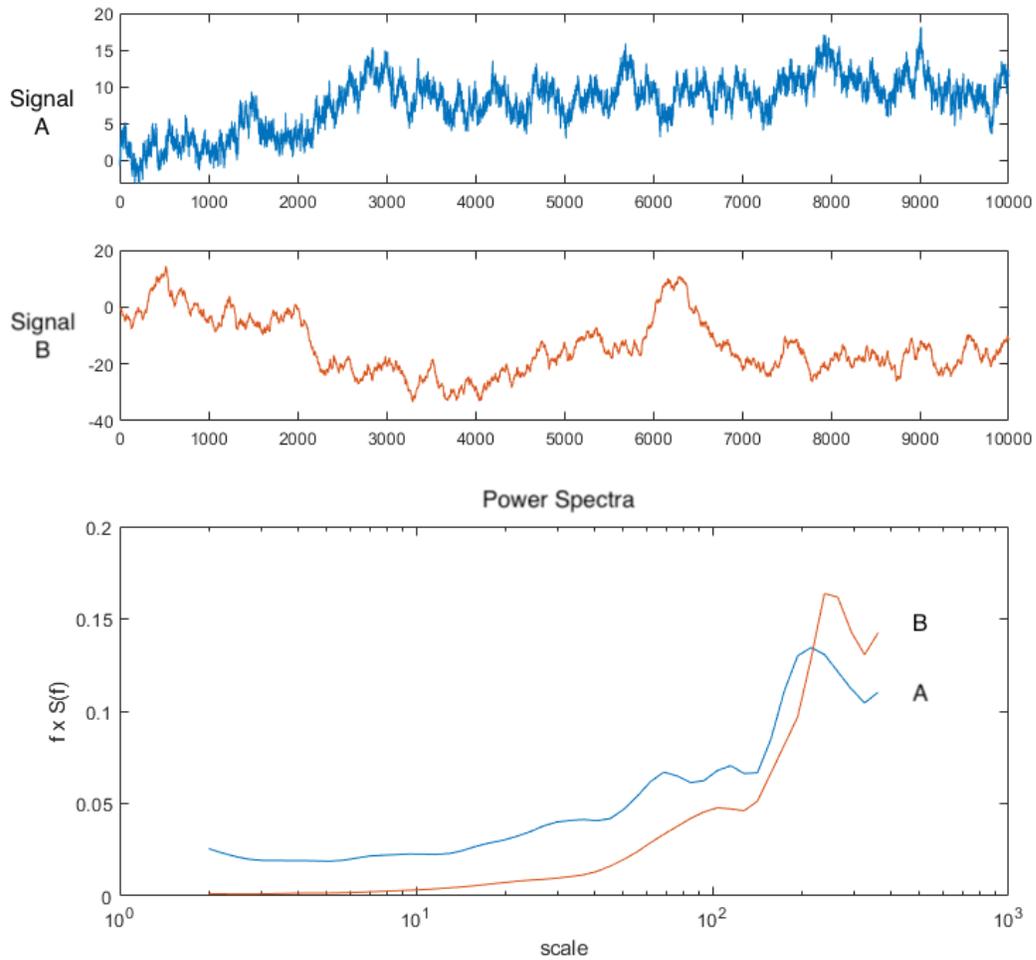
349

350 **Figure A1.** Sample signals with relatively higher noise (Signal A) and lower noise (Signal B) and their corresponding
351 Power Spectra ensemble plotted as normalized on log scale. Note the representation of the variance by area under the curve
352 is preserved by multiplying the Power (S(f)) by the frequency (f). In this way the area beneath the curve is still proportional
353 to the variance.

354
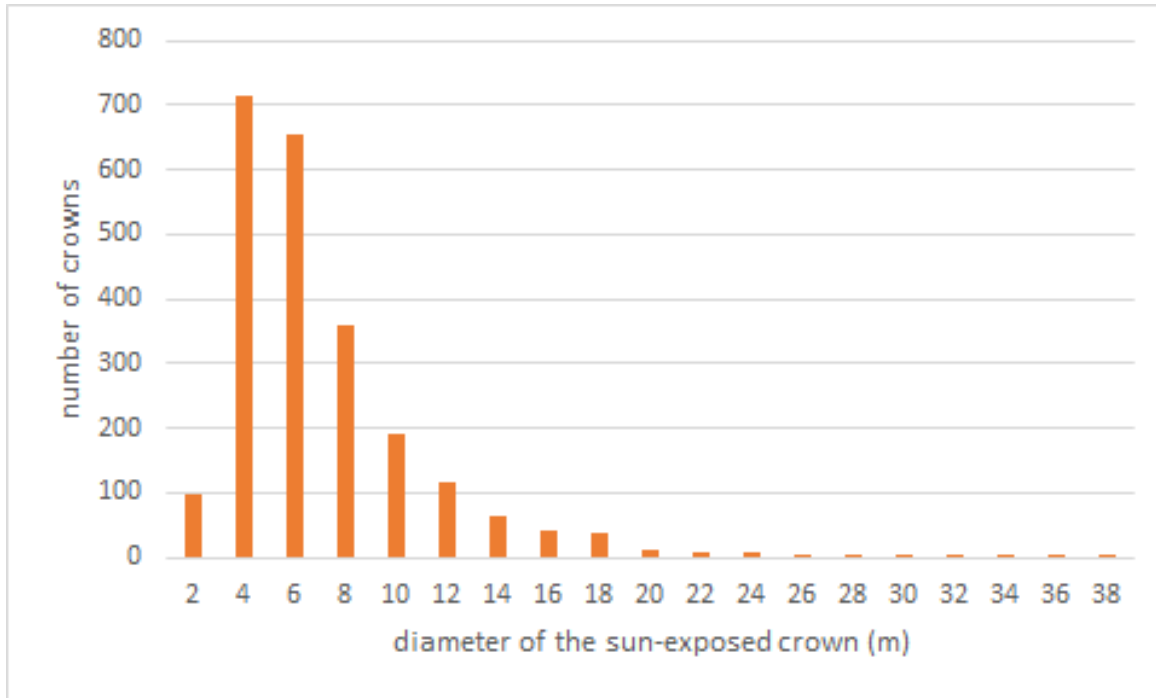
355

356 **Figure A2.** Distribution of tree crown sizes on BCI in a sample ~10 ha plot taken from digitized high spatial resolution
357 stereo photos that were linked to stems in the field (Bohlman and Pacala 2012). This ~10 ha plot does not coincide with the
358 ~10 ha area sampled by the UAS near the eddy covariance tower in this study.

359

360 **Table A1. Mean, standard deviation (Sdev) and coefficient of variation (CV) of NIRv, NIRvrad, and FCVI measurements**
361 **for the study.**

362

Flight Time	Mean NIRv	SDev NIRv	CV NIRv (%)	Mean NIRvrad	SDev NIRvrad	CV NIRvrad (%)	Mean FCVI	SDev FCVI	CV FCVI (%)
Jan30_1000	0.26	0.16	61.36	0.60	0.36	60.54	0.29	0.18	59.69
Jan30_1100	0.24	0.15	61.48	0.54	0.33	60.56	0.27	0.16	60.89
Jan30_1200	0.29	0.15	49.20	0.82	0.39	47.59	0.34	0.16	47.88
Jan30_1330	0.28	0.14	50.46	0.81	0.40	49.24	0.32	0.16	49.16
Jan30_1430	0.27	0.15	55.46	0.70	0.38	54.38	0.31	0.17	54.22
Jan30_1530	0.21	0.14	65.10	0.63	0.41	64.71	0.25	0.16	64.01
Jan30_1630	0.16	0.14	91.54	0.32	0.30	91.54	0.17	0.15	91.39
Jan31_0900	0.22	0.14	66.31	0.52	0.34	65.25	0.25	0.16	66.01
Jan31_1000	0.24	0.14	59.43	0.66	0.39	58.29	0.27	0.16	59.04
Jan31_1230	0.30	0.14	47.17	1.09	0.50	45.63	0.35	0.16	45.91
Jan31_1330	0.22	0.14	61.91	0.82	0.51	61.47	0.25	0.15	60.53
Jan31_1430	0.16	0.14	85.32	0.50	0.42	83.81	0.19	0.16	83.83

| Jan31_1530 | 0.86 | 0.08 | 9.83 | 0.61 | 0.12 | 20.24 | 0.53 | 0.04 | 8.15 |

363

364 **Table A2. Mean, standard deviation (Sdev) and coefficient of variation (CV) of NDVI and EVI measurements for the study.**

365

Flight Time	Mean NDVI	SDev NDVI	CV NDVI (%)	Mean EVI	SDev EVI	CV EVI (%)
Jan30_1000	0.86	0.10	11.64	0.57	0.18	31.54
Jan30_1100	0.88	0.09	10.15	0.57	0.14	24.40
Jan30_1200	0.85	0.09	10.38	0.52	0.15	28.48
Jan30_1330	0.85	0.09	10.60	0.59	0.15	25.24
Jan30_1430	0.85	0.09	10.35	0.61	0.16	26.84
Jan30_1530	0.85	0.11	12.52	0.54	0.19	35.21
Jan30_1630	0.93	0.06	6.69	0.49	0.18	36.90
Jan31_0900	0.87	0.10	11.54	0.51	0.19	37.24
Jan31_1000	0.87	0.10	11.08	0.55	0.19	34.66
Jan31_1230	0.85	0.08	9.82	0.66	0.15	22.72
Jan31_1330	0.85	0.09	10.70	0.55	0.19	33.80
Jan31_1430	0.85	0.09	10.58	0.42	0.18	43.07
Jan31_1530	0.86	0.08	9.83	0.61	0.12	20.24

366
367
368
369

370

371 *Code availability*

372 *Data availability*

373 GatorEye data related to this project can be downloaded from www.gatoreye.org. Code and other material
374 with links provided upon request (repository forthcoming).

375

376 *Author contributions*

377 T.M. designed the study with the help of S.P. and S.A.B.. M.D. and T.M. outfitted the tower and collected tower-
378 based data, T.M. and E.N.B. collected the UAS data. E.N.B., A.M.A.Z., and T.M. pre-processed the hyperspectral and
379 lidar data. T.M. and M.D. further processed UAV, lidar, and GPP data and ran data analysis. M.D., S.P., S.A.B., C.S.,
380 contributed with the methodological framework, data processing analysis and write up T.M., M.D., S.P., S.A.B., C.S.,

381 E.N.B., and A.M.A.Z. contributed to the interpretation, quality control and revisions of the manuscript. All authors

382 read and approved the final version of the manuscript.

383 *Competing interests*

384 The authors declare no conflict of interest.

385 *Acknowledgments*

386   Support for this project, including portions of field logistic and data collection costs and materials, and

387 support for T.M., was provided by the Provost's Postdoctoral Fellows Program at Florida State University. E.N.B.

388 was supported through the School of Forest, Fisheries and Geomatics Sciences, A.M.A.Z through the Center for Latin

389 American Studies, and hardware, software, and system costs associated with the GatorEye and data collection were

390 provided through the McIntire Stennis Program of the USDA and the School of Forest, Fisheries and Geomatics

391 Sciences. M.D. was supported by the Carbon Mitigation Initiative at Princeton University. The authors wish to thank

392 the vast support of the collaborators, staff, and researchers at the Smithsonian Tropical Research Institute and,

393 specifically at Barro Colorado Island, without which this research would not be possible. Among other contributors

394 to the work, we also extend special thanks to Alfonso Zambrano, Carli Merrick, Riley Fortier, and Pete Kerby-Miller

395 for field work assistance, and Dr. S. Joseph Wright and Dr. Helene Muller-Landau for support on site as well.

396

References

398 Alonso, L., Moreno, J., Moya, I., and R. Miller, J. R.: A Comparison of Different Techniques for Passive Measurement
399 of Vegetation Photosynthetic Activity: Solar-Induced Fluorescence, Red-Edge Reflectance Structure and
400 Photochemical Reflectance Indices, IEEE, 3, 2003.
401 Alonso, L., Gómez-Chova, L., Vila-Francés, J., Amorós-López, J., Guanter, L., Calpe, J., and Moreno, J.: Sensitivity
402 analysis of the Fraunhofer Line Discrimination method for the measurement of chlorophyll fluorescence using a field
403 spectroradiometer, IEEE, 4, 2007.
404 Alonso, L., Gómez-Chova, L., Vila-Francés, J., Amorós-López, J., Guanter, L., Calpe, J., and Moreno, J.: Improved
405 Fraunhofer Line Discrimination Method for Vegetation Fluorescence Quantification, IEEE GEOSCIENCE AND
406 REMOTE SENSING LETTERS, 5, 5, 2008.
407 Badgley, G., Field, C. B., and Berry, J. A.: Canopy near-infrared reflectance and terrestrial photosynthesis, Sci Adv,
408 3, e1602244, 10.1126/sciadv.1602244, 2017.
409 Badgley, G., Anderegg, L. D. L., Berry, J. A., and Field, C. B.: Terrestrial gross primary production: Using NIRV to
410 scale from site to globe, Glob Chang Biol, 25, 3731-3740, 10.1111/gcb.14729, 2019.
411 Baldocchi, D. D., Ryu, Y., Dechant, B., Eichelmann, E., Hemes, K., Ma, S., Rey Sanchez, C., Shortt, R., Szutu, D.,
412 Valach, A., Verfaillie, J., Badgley, G., Zeng, Y., and Berry, J. A.: Outgoing Near Infrared Radiation from Vegetation
413 Scales with Canopy Photosynthesis Across a Spectrum of Function, Structure, Physiological Capacity and Weather,
414 Journal of Geophysical Research: Biogeosciences, 10.1029/2019jg005534, 2020.
415 Berry, Z. C., & Goldsmith, G. R.: Diffuse light and wetting differentially affect tropical tree leaf photosynthesis. New
416 Phytologist, 225(1), 143-153, 10.1111/nph.16121,2020.
417 Bohlman, S. and O'Brien, S.: Allometry, adult stature and regeneration requirement of 65 tree species on Barro
418 Colorado Island, Panama, Journal of Tropical Ecology, 22, 123-136, 10.1017/s0266467405003019, 2006.
419 Bohlman, S. and Pacala, S.: A forest structure model that determines crown layers and partitions growth and mortality
420 rates for landscape-scale applications of tropical forests, Journal of Ecology, 100, 508-518, 10.1111/j.1365-
421 2745.2011.01935.x, 2012.

Castro, A. O., Chen, J., Zang, C. S., Shekhar, A., Jimenez, J. C., Bhattacharjee, S., Kindu, M., Morales, V. H., and Rammig, A.: OCO-2 Solar-Induced Chlorophyll Fluorescence Variability across Ecoregions of the Amazon Basin and the Extreme Drought Effects of El Niño (2015–2016), Remote Sensing, 12, 10.3390/rs12071202, 2020.

Clark, D. B., Olivas, P. C., Oberbauer, S. F., Clark, D. A., and Ryan, M. G.: First direct landscape-scale measurement of tropical rain forest Leaf Area Index, a key driver of global primary productivity, Ecol Lett, 11, 163-172, 10.1111/j.1461-0248.2007.01134.x, 2008.

Clark, D. A., Asao, S., Fisher, R., Reed, S., Reich, P. B., Ryan, M. G., Wood, T. E., and Yang, X.: Reviews and syntheses: Field data to benchmark the carbon cycle models for tropical forests, Biogeosciences, 14, 4663-4690, 10.5194/bg-14-4663-2017, 2017.

Cogliati, S., Verhoef, W., Kraft, S., Sabater, N., Alonso, L., Vicent, J., Moreno, J., Drusch, M., and Colombo, R.: Retrieval of sun-induced fluorescence using advanced spectral fitting methods, Remote Sensing of Environment, 169, 344-357, 10.1016/j.rse.2015.08.022, 2015.

Condit, R. S., Watts, K., Bohlman, S., Perez, R., Foster, R. B., and Hubbell, S. P.: Quantifying the deciduousness of tropical forest canopies under varying climates, Journal of Vegetation Science, 11, 10, 2000.

Dechant, B., Ryu, Y., Badgley, G., Zeng, Y., Berry, J. A., Zhang, Y., Goulas, Y., Li, Z., Zhang, Q., Kang, M., Li, J., and Moya, I.: Canopy structure explains the relationship between photosynthesis and sun-induced chlorophyll fluorescence in crops, Remote Sensing of Environment, 241, 10.1016/j.rse.2020.111733, 2020.

Detto, M., Baldocchi, D., and Katul, G. G.: Scaling Properties of Biologically Active Scalar Concentration Fluctuations in the Atmospheric Surface Layer over a Managed Peatland, Boundary-Layer Meteorology, 136, 407-430, 10.1007/s10546-010-9514-z, 2010.

Detto, M., Wright, S. J., Calderon, O., and Muller-Landau, H. C.: Resource acquisition and reproductive strategies of tropical forest in response to the El Nino-Southern Oscillation, Nature communications, 9, 913, 10.1038/s41467-018-03306-9, 2018.

Frankenberg, C., Fisher, J. B., Worden, J. R., Badgley, G., Saatchi, S. S., Lee, J. E., Toon, G. C., Butz, A., Jung, M., Kuze, A., and Yokota, T.: New global observations of the terrestrial carbon cycle from GOSAT: Patterns of plant fluorescence with gross primary productivity, Geophysical Research Letters, 38, 10.1029/2011gl048738, 2011.

Gamon, J. A., Kovalchuck, O., Wong, C. Y. S., Harris, A., and Garrity, S. R.: Monitoring seasonal and diurnal changes in photosynthetic pigments with automated PRI and NDVI sensors, Biogeosciences, 12, 4149-4159, 10.5194/bg-12-4149-2015, 2015.

Gao, W., Kim, Y., Ustin, S. L., Huete, A. R., Jiang, Z., and Miura, T.: Multisensor reflectance and vegetation index comparisons of Amazon tropical forest phenology with hyperspectral Hyperion data, Remote Sensing and Modeling of Ecosystems for Sustainability IV, 10.1117/12.734974, 2007.

Gelybó, G., Barcza, Z., Kern, A., and Kljun, N.: Effect of spatial heterogeneity on the validation of remote sensing based GPP estimations, Agricultural and Forest Meteorology, 174-175, 43-53, 10.1016/j.agrformet.2013.02.003, 2013.

Glenn, E. P., Huete, A. R., Nagler, P. L., and Nelson, S. G.: Relationship Between Remotely-sensed Vegetation Indices, Canopy Attributes and Plant Physiological Processes: What Vegetation Indices Can and Cannot Tell Us About the Landscape, Sensors, 8, 24, 2008.

Guan, K., Pan, M., Li, H., Wolf, A., Wu, J., Medvigy, D., Caylor, K. K., Sheffield, J., Wood, E. F., Malhi, Y., Liang, M., Kimball, J. S., Saleska, Scott R., Berry, J., Joiner, J., and Lyapustin, A. I.: Photosynthetic seasonality of global tropical forests constrained by hydroclimate, Nature Geoscience, 8, 284-289, 10.1038/ngeo2382, 2015.

Guanter, L., Frankenberg, C., Dudhia, A., Lewis, P. E., Gómez-Dans, J., Kuze, A., Suto, H., and Grainger, R. G.: Retrieval and global assessment of terrestrial chlorophyll fluorescence from GOSAT space measurements, Remote Sensing of Environment, 121, 236-251, 10.1016/j.rse.2012.02.006, 2012.

Guanter, L., Zhang, Y., Jung, M., Joiner, J., Voigt, M., Berry, J. A., Frankenberg, C., Huete, A. R., Zarco-Tejada, P., Lee, J. E., Moran, M. S., Ponce-Campos, G., Beer, C., Camps-Valls, G., Buchmann, N., Gianelle, D., Klumpp, K., Cescatti, A., Baker, J. M., and Griffis, T. J.: Global and time-resolved monitoring of crop photosynthesis with chlorophyll fluorescence, Proceedings of the National Academy of Sciences of the United States of America, 111, E1327-1333, 10.1073/pnas.1320008111, 2014.

Hao, D., Asrar, G. R., Zeng, Y., Yang, X., Li, X., Xiao, J., Guan, K., Wen, J., Xiao, Q., Berry, J. A., and Chen, M.: Potential of hotspot solar-induced chlorophyll fluorescence for better tracking terrestrial photosynthesis, Glob Chang Biol, 10.1111/gcb.15554, 2021.

Heinsch, F. A., Maosheng, Z., Running, S. W., Kimball, J. S., Nemani, R. R., Davis, K. J., Bolstad, P. V., Cook, B. D., Desai, A. R., Ricciuto, D. M., Law, B. E., Oechel, W. C., Hyojung, K., Hongyan, L., Wofsy, S. C., Dunn, A. L., Munger, J. W., Baldocchi, D. D., Liukang, X., Hollinger, D. Y., Richardson, A. D., Stoy, P. C., Siqueira, M. B. S., Monson, R. K., Burns, S. P., and Flanagan, L. B.: Evaluation of remote sensing based terrestrial productivity from

478 MODIS using regional tower eddy flux network observations, IEEE Transactions on Geoscience and Remote Sensing,
479 44, 1908-1925, 10.1109/tgrs.2005.853936, 2006.

480 Huete, A., Didan, K., Miura, T., Rodriguez, E. P., Gao, X., and Ferreira, L. G.: Overview of the radiometric and
481 biophysical performanceof the MODIS vegetation indices, Remote Sensing of Environment, 83, 19, 2002.

482 Huete, A. R., Restrepo-Coupe, N., Ratana, P., Didan, K., Saleska, S. R., Ichii, K., Panuthai, S., and Gamo, M.: Multiple
483 site tower flux and remote sensing comparisons of tropical forest dynamics in Monsoon Asia, Agricultural and Forest
484 Meteorology, 148, 748-760, 10.1016/j.agrformet.2008.01.012, 2008.

485 Jiang, Z., Huete, A., Didan, K., and Miura, T.: Development of a two-band enhanced vegetation index without a blue
486 band, Remote Sensing of Environment, 112, 3833-3845, 10.1016/j.rse.2008.06.006, 2008.

487 Joiner, J., Yoshida, Y., Vasilkov, A. P., Yoshida, Y., Corp, L. A., and Middleton, E. M.: First observations of global
488 and seasonal terrestrial chlorophyll fluorescence from space, Biogeosciences, 8, 637-651, 10.5194/bg-8-637-2011,
489 2011.

490 Julitta, T.: Optical proximal sensing for vegetation monitoring, PhD Dissertation, Department of Earth and
491 Environmental Sciences, University of Milano-Bicocca, 136 pp., 2015.

492 Jung, M., Reichstein, M., Margolis, H. A., Cescatti, A., Richardson, A. D., Arain, M. A., Arneth, A., Bernhofer, C.,
493 Bonal, D., Chen, J., Gianelle, D., Gobron, N., Kiely, G., Kutsch, W., Lasslop, G., Law, B. E., Lindroth, A., Merbold,
494 L., Montagnani, L., Moors, E. J., Papale, D., Sottocornola, M., Vaccari, F., and Williams, C.: Global patterns of land-
495 atmosphere fluxes of carbon dioxide, latent heat, and sensible heat derived from eddy covariance, satellite, and
496 meteorological observations, Journal of Geophysical Research, 116, 10.1029/2010jg001566, 2011.

497 Köhler, P., Guanter, L., Kobayashi, H., Walther, S., and Yang, W.: Assessing the potential of sun-induced fluorescence
498 and the canopy scattering coefficient to track large-scale vegetation dynamics in Amazon forests, Remote Sensing of
499 Environment, 769-785, 10.1016/j.rse.2017.09.025, 2017.

500 Lasslop, G., Reichstein, M., Detto, M., Richardson, A. D., and Baldocchi, D. D.: Comment on Vickers et al.: Self-
501 correlation between assimilation and respiration resulting from flux partitioning of eddy-covariance CO_2 fluxes,
502 Agricultural and Forest Meteorology, 150, 312-314, 10.1016/j.agrformet.2009.11.003, 2010.

503 Laurance, W. F., Useche, D. C., Rendeiro, J., Kalka, M., Bradshaw, C. J., Sloan, S. P., Laurance, S. G., Campbell, M.,
504 Abernethy, K., Alvarez, P., Arroyo-Rodriguez, V., Ashton, P., Benitez-Malvido, J., Blom, A., Bobo, K. S., Cannon,
505 C. H., Cao, M., Carroll, R., Chapman, C., Coates, R., Cords, M., Danielsen, F., De Dijn, B., Dinerstein, E., Donnelly,
506 M. A., Edwards, D., Edwards, F., Farwig, N., Fashing, P., Forget, P. M., Foster, M., Gale, G., Harris, D., Harrison,
507 R., Hart, J., Karpanty, S., Kress, W. J., Krishnaswamy, J., Logsdon, W., Lovett, J., Magnusson, W., Maisels, F.,
508 Marshall, A. R., McClearn, D., Mudappa, D., Nielsen, M. R., Pearson, R., Pitman, N., van der Ploeg, J., Plumptre, A.,
509 Poulsen, J., Quesada, M., Rainey, H., Robinson, D., Roetgers, C., Rovero, F., Scatena, F., Schulze, C., Sheil, D.,
510 Struhsaker, T., Terborgh, J., Thomas, D., Timm, R., Urbina-Cardona, J. N., Vasudevan, K., Wright, S. J., Arias, G. J.,
511 Arroyo, L., Ashton, M., Auzel, P., Babaasa, D., Babweteera, F., Baker, P., Banki, O., Bass, M., Bila-Isia, I., Blake,
512 S., Brockelman, W., Brokaw, N., Bruhl, C. A., Bunyavejchewin, S., Chao, J. T., Chave, J., Chellam, R., Clark, C. J.,
513 Clavijo, J., Congdon, R., Corlett, R., Dattaraja, H. S., Dave, C., Davies, G., Beisiegel Bde, M., da Silva Rde, N., Di
514 Fiore, A., Diesmos, A., Dirzo, R., Doran-Sheehy, D., Eaton, M., Emmons, L., Estrada, A., Ewango, C., Fedigan, L.,
515 Feer, F., Fruth, B., Willis, J. G., Goodale, U., Goodman, S., Guix, J. C., Guthiga, P., Haber, W., Hamer, K., Herbinger,
516 I., Hill, J., Huang, Z., Sun, I. F., Ickes, K., Itoh, A., Ivanauskas, N., Jackes, B., Janovec, J., Janzen, D., Jiangming, M.,
517 Jin, C., Jones, T., Justiniano, H., Kalko, E., Kasangaki, A., Killeen, T., King, H. B., Klop, E., Knott, C., Kone, I.,
518 Kudavidanage, E., Ribeiro, J. L., Lattke, J., Laval, R., Lawton, R., Leal, M., Leighton, M., Lentino, M., Leonel, C.,
519 Lindsell, J., Ling-Ling, L., Linsenmair, K. E., Losos, E., Lugo, A., Lwanga, J., Mack, A. L., Martins, M., McGraw,
520 W. S., McNab, R., Montag, L., Thompson, J. M., Nabe-Nielsen, J., Nakagawa, M., Nepal, S., Norconk, M., Novotny,
521 V., O'Donnell, S., Opiang, M., Ouboter, P., Parker, K., Parthasarathy, N., Pisciotta, K., Prawiradilaga, D., Pringle, C.,
522 Rajathurai, S., Reichard, U., Reinartz, G., Renton, K., Reynolds, G., Reynolds, V., Riley, E., Rodel, M. O., Rothman,
523 J., Round, P., Sakai, S., Sanaiotti, T., Savini, T., Schaab, G., Seidensticker, J., Siaka, A., Silman, M. R., Smith, T. B.,
524 de Almeida, S. S., Sodhi, N., Stanford, C., Stewart, K., Stokes, E., Stoner, K. E., Sukumar, R., Surbeck, M., Tobler,
525 M., Tscharntke, T., Turkalo, A., Umapathy, G., van Weerd, M., Rivera, J. V., Venkataraman, M., Venn, L., Verea,
526 C., de Castilho, C. V., Waltert, M., Wang, B., Watts, D., Weber, W., West, P., Whitacre, D., Whitney, K., Wilkie, D.,
527 Williams, S., Wright, D. D., Wright, P., Xiankai, L., Yonzon, P., and Zamzani, F.: Averting biodiversity collapse in
528 tropical forest protected areas, Nature, 489, 290-294, 10.1038/nature11318, 2012.

529 Lee, J. E., Frankenberg, C., van der Tol, C., Berry, J. A., Guanter, L., Boyce, C. K., Fisher, J. B., Morrow, E., Worden,
530 J. R., Asefi, S., Badgley, G., and Saatchi, S.: Forest productivity and water stress in Amazonia: observations from
531 GOSAT chlorophyll fluorescence, Proceedings. Biological sciences / The Royal Society, 280, 20130171,
532 10.1098/rspb.2013.0171, 2013.

Lewis, S. L., Lloyd, J., Sitch, S., Mitchard, E. T. A., and Laurance, W. F.: Changing Ecology of Tropical Forests: Evidence and Drivers, Annual Review of Ecology, Evolution, and Systematics, 40, 529-549, 10.1146/annurev.ecolsys.39.110707.173345, 2009.

Liangyun Liu, X. L., ZhihuiWang, and Bing Zhang: Measurement and Analysis of BidirectionalSIF Emissions in Wheat Canopies, IEEE TRANSACTIONS ON GEOSCIENCE AND REMOTE SENSING, 12, 2016.

Liu, J., Bowman, K. W., Schimel, D. S., Parazoo, N. C., Jiang, Z., Lee, M., Bloom, A. A., Wunch, D., Frankenberg, C., Sun, Y., O'Dell, C. W., Gurney, K. R., Menemenlis, D., Gierach, M., Crisp, D., and Eldering, A.: Contrasting carbon cycle responses of the tropical continents to the 2015-2016 El Nino, Science, 358, eaam5690, 10.1126/science.aam5690, 2017.

Liu, L., Yang, X., Gong, F., Su, Y., Huang, G., and Chen, X.: The Novel Microwave Temperature Vegetation Drought Index (MTVDI) Captures Canopy Seasonality across Amazonian Tropical Evergreen Forests, Remote Sensing, 13, 10.3390/rs13030339, 2021.

Liu, X., Liu, L., Zhang, S., and Zhou, X.: New Spectral Fitting Method for Full-Spectrum Solar-Induced Chlorophyll Fluorescence Retrieval Based on Principal Components Analysis, Remote Sensing, 7, 10626-10645, 10.3390/rs70810626, 2015.

Logan, B. A., Adams, W. W., and Demmig-Adams, B.: Viewpoint:Avoiding common pitfalls of chlorophyll fluorescence analysis under field conditions, Functional Plant Biology, 34, 853, 10.1071/fp07113, 2007.

Magney, T. S., Frankenberg, C., Fisher, J. B., Sun, Y., North, G. B., Davis, T. S., Kornfeld, A., and Siebke, K.: Connecting active to passive fluorescence with photosynthesis: a method for evaluating remote sensing measurements of Chl fluorescence, The New phytologist, 1594-1608, 10.1111/nph.14662, 2017.

Malenovsky, Z., Mishra, K. B., Zemek, F., Rascher, U., and Nedbal, L.: Scientific and technical challenges in remote sensing of plant canopy reflectance and fluorescence, Journal of experimental botany, 60, 2987-3004, 10.1093/jxb/erp156, 2009.

Malhi, Y.: The productivity, metabolism and carbon cycle of tropical forest vegetation, Journal of Ecology, 100, 65-75, 10.1111/j.1365-2745.2011.01916.x, 2012.

Medlyn, B. E.: Physiological basis of the light use efficiency model, Tree Physiology, 18, 167–176, https://doi.org/10.1093/treephys/18.3.167, 1998.

Meroni, M., Rossini, M., Guanter, L., Alonso, L., Rascher, U., Colombo, R., and Moreno, J.: Remote sensing of solar-induced chlorophyll fluorescence: Review of methods and applications, Remote Sensing of Environment, 113, 2037-2051, 10.1016/j.rse.2009.05.003, 2009.

Merrick, Pau, Jorge, Bennartz, and Silva: Spatiotemporal Patterns and Phenology of Tropical Vegetation Solar-Induced Chlorophyll Fluorescence across Brazilian Biomes Using Satellite Observations, Remote Sensing, 11, 10.3390/rs11151746, 2019.

Merrick, T., Jorge, M. L. S. P., Silva, T. S. F., Pau, S., Rausch, J., Broadbent, E. N., and Bennartz, R.: Characterization of chlorophyll fluorescence, absorbed photosynthetically active radiation, and reflectance-based vegetation index spectroradiometer measurements, International Journal of Remote Sensing, 41, 6755-6782, 10.1080/01431161.2020.1750731, 2020.

Mitchard, E. T. A.: The tropical forest carbon cycle and climate change, Nature, 559, 527-534, 10.1038/s41586-018-0300-2, 2018.

Monteith, J.L., Climate and the efficiency of crop production in Britain, Phil. Trans. R. Soc. Land., 281, 277-294, 1977.

Morton, D. C., Rubio, J., Cook, B. D., Gastellu-Etchegorry, J. P., Longo, M., Choi, H., Hunter, M. O., and Keller, M.: Amazon forest structure generates diurnal and seasonal variability in light utilization, Biogeosciences Discussions, 12, 19043-19072, 10.5194/bgd-12-19043-2015, 2015.

Morton, D. C., Nagol, J., Carabajal, C. C., Rosette, J., Palace, M., Cook, B. D., Vermote, E. F., Harding, D. J., and North, P. R.: Amazon forests maintain consistent canopy structure and greenness during the dry season, Nature, 506, 221-224, 10.1038/nature13006, 2014.

Moya, I., Camenen, L., Evain, S., Goulas, Y., Cerovic, Z. G., Latouche, G., Flexas, J., and Ounis, A.: A new instrument for passive remote sensing1. Measurements of sunlight-induced chlorophyll fluorescence, Remote Sensing of Environment, 91, 186-197, 10.1016/j.rse.2004.02.012, 2004.

Plascyk, J. A.: The MK II Fraunhofer Line Discriminator (FLD -II) for Airborne and Orbital Remote Sensing of Solar-Stimulated Luminescense, Optical Engineering, 14, 8, 1975.

Porcar-Castell, A., Tyystjarvi, E., Atherton, J., van der Tol, C., Flexas, J., Pfundel, E. E., Moreno, J., Frankenberg, C., and Berry, J. A.: Linking chlorophyll a fluorescence to photosynthesis for remote sensing applications: mechanisms and challenges, Journal of experimental botany, 65, 4065-4095, 10.1093/jxb/eru191, 2014.

R Development Core Team: R: A language and environment for statistical computing, R Foundation for Statistical Computing [code], 2010.

Rocha, A. V., Appel, R., Bret-Harte, M. S., Euskirchen, E. S., Salmon, V., and Shaver, G.: Solar position confounds the relationship between ecosystem function and vegetation indices derived from solar and photosynthetically active radiation fluxes, Agricultural and Forest Meteorology, 298-299, 10.1016/j.agrformet.2020.108291, 2021.

Rong Li, F. Z.: Accuracy assessment on reconstruction algorithms of solar-induced Fluorescence Spectrum, Geoscience and Remote Sensing Symposium (IGARSS) IEEE International, 1727-1730,

Rossini, M., Alonso, L., Cogliati, S., Damm, A., Guanter, L., Julitta, T., Meroni, M., Moreno, J., Panigada, C., Pinto, F., Rascher, U., Schickling, A., Schüttemeyer, D., Zemek, F., and Colombo, R.: Measuring sun-induced chlorophyll fluorescence: An evaluation and synthesis of existing field data, 5th International workshop on remote sensing of vegetation fluorescence, Paris, France, 1-5,

Rouse Jr, J. W., Haas, R. H., Schell, J. A., and Deering, D. W.: Paper A 20, hird Earth Resources Technology Satellite-1 Symposium: The Proceedings of a Symposium Goddard Space Flight Center at Washington, DC 309,

Running, S. W., Nemani, R. R., Heinsch, F. A., Zhao, M., Reeves, M., and Hashimoto, H.: A Continuous Satellite-Derived Measure of Global Terrestrial Primary Production, BioScience, 54, 547-551, 2004.

Ryu, Y., Jiang, C., Kobayashi, H., and Detto, M.: MODIS-derived global land products of shortwave radiation and diffuse and total photosynthetically active radiation at 5 km resolution from 2000, Remote Sensing of Environment, 204, 812-825, 10.1016/j.rse.2017.09.021, 2018.

Saatchi, S. S., Harris, N. L., Brown, S., Lefsky, M. A., E. T., Mitchare, W. S., Zutta, B. R., Buerman, W., Lewis, S. L., Hagen, S., Petrova, S., White, L., Silman, M., and Morel, A.: Benchmark map of forest carbon stocks in tropical regions across three continents, Proceedings of the National Academy of Sciences, 108, 9899-9905, 2010.

Saatchi, S. S., Harris, N. L., Brown, S., Lefsky, M., Mitchard, E. T., Salas, W., Zutta, B. R., Buermann, W., Lewis, S. L., Hagen, S., Petrova, S., White, L., Silman, M., and Morel, A.: Benchmark map of forest carbon stocks in tropical regions across three continents, Proceedings of the National Academy of Sciences of the United States of America, 108, 9899-9904, 10.1073/pnas.1019576108, 2011.

Samanta, A., Ganguly, S., and Myneni, R.: MODIS Enhanced Vegetation Index data do not show greening of Amazon forests during the 2005 drought, New Phytologist, 189, 4, 2010.

Schickling, A., Matveeva, M., Damm, A., Schween, J., Wahner, A., Graf, A., Crewell, S., and Rascher, U.: Combining Sun-Induced Chlorophyll Fluorescence and Photochemical Reflectance Index Improves Diurnal Modeling of Gross Primary Productivity, Remote Sensing, 8, 574, 10.3390/rs8070574, 2016.

Sims, D., Rahman, A., Cordova, V., Elmasri, B., Baldocchi, D., Bolstad, P., Flanagan, L., Goldstein, A., Hollinger, D., and Misson, L.: A new model of gross primary productivity for North American ecosystems based solely on the enhanced vegetation index and land surface temperature from MODIS, Remote Sensing of Environment, 112, 1633-1646, 10.1016/j.rse.2007.08.004, 2008.

Springer, K., Wang, R., and Gamon, J. A.: Parallel Seasonal Patterns of Photosynthesis, Fluorescence, and Reflectance Indices in Boreal Trees, Remote Sensing, 9, 1-18, 10.3390/rs9070691, 2017.

Sun, Y., Frankenberg, C., Wood, J. D., Schimel, D. S., Jung, M., Guanter, L., Drewry, D. T., Verma, M., Porcar-Castell, A., Griffis, T. J., Gu, L., Magney, T. S., Kohler, P., Evans, B., and Yuen, K.: OCO-2 advances photosynthesis observation from space via solar-induced chlorophyll fluorescence, Science, 358, eaam5747, 10.1126/science.aam5747, 2017.

Torrence, C. and Compo, G. P.: A Practical Guide to Wavelet Analysis, Bulletin of the American Meteorological Society, 79, 61-79, 1998.

Tucker, C., Red and photographic infrared linear combinations for vegetation monitoring, Remote Sensing of Environment, 8, 127-150,1979.

Turner, D. P., Ritts, W. D., Cohen, W. B., Gower, S. T., Zhao, M., Running, S. W., Wofsy, S. C., Urbanski, S., Dunn, A. L., and Munger, J. W.: Scaling Gross Primary Production (GPP) over boreal and deciduous forest landscapes in support of MODIS GPP product validation, Remote Sensing of Environment, 88, 256-270, 10.1016/j.rse.2003.06.005, 2003.

Van Wittenberghe, S., Alonso, L., Verrelst, J., Moreno, J., and Samson, R.: Bidirectional sun-induced chlorophyll fluorescence emission is influenced by leaf structure and light scattering properties — A bottom-up approach, Remote Sensing of Environment, 158, 169-179, 10.1016/j.rse.2014.11.012, 2015.

Van Wittenberghe, S., Alonso, L., Verrelst, J., Hermans, I., Delegido, J., Veroustraete, F., Valcke, R., Moreno, J., and Samson, R.: Upward and downward solar-induced chlorophyll fluorescence yield indices of four tree species as indicators of traffic pollution in Valencia, Environmental pollution, 173, 29-37, 10.1016/j.envpol.2012.10.003, 2013.

Wang, C., Beringer, J., Hutley, L. B., Cleverly, J., Li, J., Liu, Q., and Sun, Y.: Phenology Dynamics of Dryland Ecosystems Along the North Australian Tropical Transect Revealed by Satellite Solar-Induced Chlorophyll Fluorescence, Geophysical Research Letters, 46, 5294-5302, 10.1029/2019gl082716, 2019.

Wang, S., Zhang, Y., Ju, W., Qiu, B., and Zhang, Z.: Tracking the seasonal and inter-annual variations of global gross primary production during last four decades using satellite near-infrared reflectance data, The Science of the total environment, 755, 142569, 10.1016/j.scitotenv.2020.142569, 2020.

Wickham, H.: ggplot2: Elegant Graphics for Data Analysis, Springer-Verlag [code], 2016.

Wickham, H.: tidyverse: Easily Install and Load the 'Tidyverse' (R package version 1.2.1) [code], 2017.

Wickham, H., François, R., Henry, L., and Müller, K.: dplyr: A Grammar of Data Manipulation (R package version 0.7.8) [code], 2018.

Wright, S. J.: The future of tropical forests, Ann N Y Acad Sci, 1195, 1-27, 10.1111/j.1749-6632.2010.05455.x, 2010.

Wu, G., Guan, K., Jiang, C., Peng, B., Kimm, H., Chen, M., Yang, X., Wang, S., Suyker, A. E., Bernacchi, C. J., Moore, C. E., Zeng, Y., Berry, J. A., and Cendrero-Mateo, M. P.: Radiance-based NIRv as a proxy for GPP of corn and soybean, Environmental Research Letters, 15, 10.1088/1748-9326/ab65cc, 2020.

Xu, L., Saatchi, S. S., Yang, Y., Myneni, R. B., Frankenberg, C., Chowdhury, D., and Bi, J.: Satellite observation of tropical forest seasonality: spatial patterns of carbon exchange in Amazonia, Environmental Research Letters, 10, 084005, 10.1088/1748-9326/10/8/084005, 2015.

Yang, H., Yang, X., Zhang, Y., Heskel, M. A., Lu, X., Munger, J. W., Sun, S., and Tang, J.: Chlorophyll fluorescence tracks seasonal variations of photosynthesis from leaf to canopy in a temperate forest, Glob Chang Biol, 23, 2874-2886, 10.1111/gcb.13590, 2017.

Yang, J., Tian, H., Pan, S., Chen, G., Zhang, B., and Dangal, S.: Amazon droughts and forest responses: Largely reduced forest photosynthesis but slightly increased canopy greenness during the extreme drought of 2015/2016, Glob Chang Biol, 1919-1934, 10.1111/gcb.14056, 2018a.

Yang, K., Ryu, Y., Dechant, B., Berry, J. A., Hwang, Y., Jiang, C., Kang, M., Kim, J., Kimm, H., Kornfeld, A., and Yang, X.: Sun-induced chlorophyll fluorescence is more strongly related to absorbed light than to photosynthesis at half-hourly resolution in a rice paddy, Remote Sensing of Environment, 216, 658-673, 10.1016/j.rse.2018.07.008, 2018b.

Yang, P., van der Tol, C., Campbell, P. K. E., and Middleton, E. M.: Fluorescence Correction Vegetation Index (FCVI): A physically based reflectance index to separate physiological and non-physiological information in far-red sun-induced chlorophyll fluorescence, Remote Sensing of Environment, 240, 10.1016/j.rse.2020.111676, 2020.

Yuan, W., Cai, W., Xia, J., Chen, J., Liu, S., Dong, W., Merbold, L., Law, B., Arain, A., Beringer, J., Bernhofer, C., Black, A., Blanken, P. D., Cescatti, A., Chen, Y., Francois, L., Gianelle, D., Janssens, I. A., Jung, M., Kato, T., Kiely, G., Liu, D., Marcolla, B., Montagnani, L., Raschi, A., Roupsard, O., Varlagin, A., and Wohlfahrt, G.: Global comparison of light use efficiency models for simulating terrestrial vegetation gross primary production based on the LaThuile database, Agricultural and Forest Meteorology, 192–193, 108–120, https://doi.org/10.1016/j.agrformet.2014.03.007, 2014.

Zarco-Tejada, P. J., González-Dugo, V., and Berni, J. A. J.: Fluorescence, temperature and narrow-band indices acquired from a UAV platform for water stress detection using a micro-hyperspectral imager and a thermal camera, Remote Sensing of Environment, 117, 322-337, 10.1016/j.rse.2011.10.007, 2012.

Zarco-Tejada, P. J., Morales, A., Testi, L., and Villalobos, F. J.: Spatio-temporal patterns of chlorophyll fluorescence and physiological and structural indices acquired from hyperspectral imagery as compared with carbon fluxes measured with eddy covariance, Remote Sensing of Environment, 133, 102-115, 10.1016/j.rse.2013.02.003, 2013.

Zarco-Tejada, P. J., Miller, J. R., Mohammed, G. H., Noland, T. L., and Sampson, P. H.: Estimation of chlorophyll fluorescence under natural illumination from hyperspectral data, International Journal of Applied Earth Observation and Geoinformation, 3, 7, 2001.

Zeng, Y., Badgley, G., Dechant, B., Ryu, Y., Chen, M., and Berry, J. A.: A practical approach for estimating the escape ratio of near-infrared solar-induced chlorophyll fluorescence, Remote Sensing of Environment, 232, 10.1016/j.rse.2019.05.028, 2019.

Zhang, Z., Zhang, Y., Zhang, Q., Chen, J. M., Porcar-Castell, A., Guanter, L., Wu, Y., Zhang, X., Wang, H., Ding, D., and Li, Z.: Assessing bi-directional effects on the diurnal cycle of measured solar-induced chlorophyll fluorescence in crop canopies, Agricultural and Forest Meteorology, 295, 10.1016/j.agrformet.2020.108147, 2020.

Zhang, Z., Zhang, Y., Zhang, Y., Gobron, N., Frankenberg, C., Wang, S., and Li, Z.: The potential of satellite FPAR product for GPP estimation: An indirect evaluation using solar-induced chlorophyll fluorescence, Remote Sensing of Environment, 240, 10.1016/j.rse.2020.111686, 2020.

697   Zhao, M., Running, S., Heinsch, F. A., and Nemani, R.: MODIS-Derived Terrestrial Primary Production, 11, 635-
698   660, 10.1007/978-1-4419-6749-7_28, 2010.
699   Zhu, X. and Liu, D.: Improving forest aboveground biomass estimation using seasonal Landsat NDVI time-series,
700   ISPRS Journal of Photogrammetry and Remote Sensing, 102, 222-231, 10.1016/j.isprsjprs.2014.08.014, 2015.
701
702